



Cite this: *RSC Adv.*, 2020, **10**, 31758

Received 30th May 2020  
 Accepted 1st August 2020

DOI: 10.1039/d0ra04770h  
[rsc.li/rsc-advances](http://rsc.li/rsc-advances)

## 2-D organization of silica nanoparticles on gold surfaces: CO<sub>2</sub> marker detection and storage†

Eduardo José Cueto Díaz,<sup>a</sup> Santos Gálvez-Martínez,<sup>a</sup> M<sup>a</sup> Carmen Torquemada Vico,<sup>b</sup> María Pilar Valles González<sup>c</sup> and Eva Mateo-Martí<sup>a</sup>

A single layer of silica nanoparticles with an average size of ~200 nm was deposited over the surface of pristine gold wafers, aided by (3-mercaptopropyl)trimethoxysilane. The nanoparticle immobilization was driven by covalent bonding rather than a self-assembly process, leading to a cluster-assembled material which has CO<sub>2</sub> sensing features. Here, we show how this device can be used for CO<sub>2</sub> physisorption and chemisorption. We analyse the device, both spectroscopically and morphologically, before and after exposure to an atmosphere of 7 mbar of CO<sub>2</sub>, inside a planetary atmospheres and surfaces simulation chamber, (PASC) mimicking Martian atmospheric conditions. Our studies demonstrate that these clusters are suitable for CO<sub>2</sub> detection and storage, under well controlled experimental Martian conditions. Their high sensitivity at a very low concentration of CO<sub>2</sub>, 12.4 ppm, makes them ideal candidates in the nanosensor field.

### 1. Introduction

CO<sub>2</sub> detection is crucial in biological, agricultural, food, medical and environmental industries,<sup>1–4</sup> and planetary science. CO<sub>2</sub> is also known as a greenhouse gas, as it absorbs and re-emits IR radiation, increasing the average temperature on earth. It is industrially employed for agricultural fumigation and for experimental plant growth. When mixed with oxygen it forms carbogen, which is used to stimulate breathing in the treatment of respiratory disease, and to increase subsurface oil recovery, and it is also widely used in carbonated drinks. Therefore, CO<sub>2</sub> gas sensing is often required to guarantee compliance with environmental laws and regulations. In particular, carbon dioxide monitoring is required in the working environment, as an abnormal high level of CO<sub>2</sub> is associated with sick building syndrome. Nowadays, CO<sub>2</sub> sensors are based on IR adsorption or electrochemical interactions that measure resistance or current.<sup>5–7</sup> Devices using such technology have an important drawback as they typically suffer from a high cross sensitivity to other gases and have poor temperature stability. At present, there is interest in the development of alternative solutions, materials with treatments that can capture CO<sub>2</sub> and/or show sensitivity to CO<sub>2</sub>. We have focused

our attention on nanoparticle-based CO<sub>2</sub> sensors, as a promising alternative for certain applications. However, the preparation of materials with nanoparticles can still be challenging due to their tendency to self-organize when deposited on thin films and the sensitivity of these procedures to various parameters.<sup>8</sup> It is the purpose of this work to describe a procedure for fabrication of CO<sub>2</sub> adsorbing surfaces, after deposition of nanoparticles on a linker film. As an example, the response of these nanoparticle clusters is here demonstrated after exposure to a pure CO<sub>2</sub> Martian-like atmosphere.

Nanoparticles (NPs) exhibit unique chemical, physical and electronic properties that are different from those of bulk materials, they indeed own outstanding catalytic, thermal and optical properties as well as robust mechanical strength and a large surface-to-volume, making them good candidates to construct sensing devices, based on clustered-nanoparticles. Although CO<sub>2</sub> nanoparticle based sensors have been mentioned in the literature during the last decades,<sup>9–11</sup> they have been barely implemented and developed for practical applications as they require a complex nanoparticle deposition set-up, which most of the times leads to either NP-aggregates<sup>12</sup> or multilayers.<sup>13</sup>

Silica NPs, (SiO<sub>2</sub>NPs) in solid state, have never been investigated as a potential CO<sub>2</sub> sensing agent. There is only one work in this regard but implemented as a colloidal solution,<sup>14</sup> others, were devoted to incorporate amine derivatives<sup>15,16</sup> over their surface taking advantage of the well-known CO<sub>2</sub> capture properties in liquid phase of amine derivatives such as: monoethanolamine (MEA), diethanolamine (DEA), diisopropanolamine (DIPA) *etc.* However, materials/polymers bearing amine groups, in practice, suffer from poisoning with carbamates and fail to fill the gap in the CO<sub>2</sub> sensor sector.<sup>17,18</sup>

<sup>a</sup>Centro de Astrobiología (CSIC-INTA), Ctra. Ajalvir, Km. 4, 28850 Torrejón de Ardoz, Madrid, Spain. E-mail: mateome@cab.inta-csic.es

<sup>b</sup>National Institute of Aerospace Technology (INTA), Department of Payloads and Space Sciences, Ctra. Torrejón-Ajalvir, 28850, Torrejón de Ardoz, Spain

<sup>c</sup>National Institute of Aerospace Technology (INTA), Materials and Structures Department, Ctra. Torrejón-Ajalvir, 28850, Torrejón de Ardoz, Spain

† Electronic supplementary information (ESI) available. See DOI: 10.1039/d0ra04770h



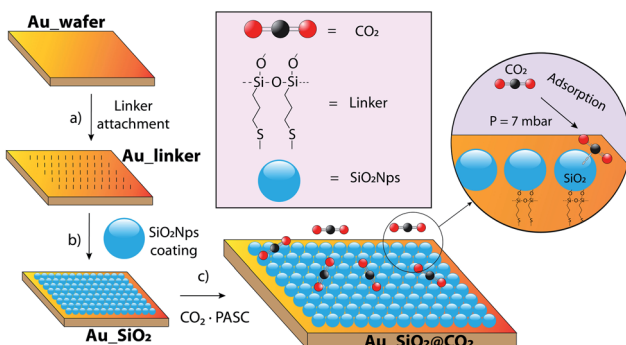


Fig. 1 Schematic representation of the  $\text{SiO}_2\text{NPs}$  deposition onto Au wafers and the subsequent  $\text{CO}_2$  adsorption process.

In this work we proposed to use silica nanoparticles ( $\text{SiO}_2\text{NPs}$ ) of 200 nm size. This is a popular material in the biomedicine field. Furthermore, they are inexpensive, and this can open new routes in the field of space and planetary exploration.  $\text{SiO}_2\text{NPs}$  also benefit from several advantages, *e.g.*, high surface area, synthetic modularity, particle size tunability *via* sol-gel process,<sup>19,20</sup> geometry and porosity control, and its demonstrated  $\text{CO}_2$  adsorption capacities in suspension (nanofluids),<sup>21</sup> all of them suggesting their potential application as a non-liquid adsorbent material, a feature barely investigated for this particular goal. Thus, here we aim to demonstrate the formation of cluster-assembled films, by the self-organization of  $\text{SiO}_2\text{NPs}$  on gold surfaces, to elucidate whether non-mesoporous silica structures are suitable as  $\text{CO}_2$  adsorber at standard Mars atmosphere conditions of 7 mbar (12.4 ppm of  $\text{CO}_2$  inside the planetary environment simulating chamber PASC<sup>22</sup>). If successful, this nanotechnology may have interest for the fixation of organic molecules and for the detection of bio-signatures in future Martian missions.<sup>23</sup> We shall next demonstrate the two-dimensional organization of silica nanoparticles on gold surfaces and characterize spectroscopically their  $\text{CO}_2$  fixation signatures. Our methodological approach is depicted in Fig. 1 and encompasses a bottom-up approach where a bare gold wafer ( $11 \times 11 \times 1$  mm) is treated with a molecular linker that is incorporating both a thiol and an ethoxysilane group, at the extremes of a propyl chain. This linker acts as a “glue” between the  $\text{SiO}_2\text{NPs}$  and the gold wafer surface (Au-linker, Fig. 1a). In a step further (Au<sub>SiO<sub>2</sub></sub>, Fig. 1b) the wafer was placed in the 200 nm size  $\text{SiO}_2\text{NPs}$  colloidal suspension (1 wt%) at different dipping time conditions. After exhaustively rinsing with water, a  $\text{SiO}_2\text{NPs}$  single monolayer (this is confirmed later on using microscopy techniques) was obtained. Finally (Au<sub>SiO<sub>2</sub></sub>@CO<sub>2</sub>, Fig. 1c),  $\text{CO}_2$  adsorption experiments were conducted under specific conditions inside the Planetary Atmospheres and Surfaces Simulation Chamber (PASC, Fig. S1†).<sup>22</sup>

## 2. Experimental

### 2.1. Nanosensor design and chemistry

The design of the sensor resulted from the idea of producing a material, which can be tailored to exhibit new collective properties which differ from those of their individual components.

The proposed strategy combines in the same chip, (i) the covalent attachment of monodispersed silica nanoparticles to (ii) an excellent conductor of electricity (Au), a material that promotes covalent bonding (Au-Si) between nanoparticles and the surface of the wafer. The gold wafers, Au (111) were manufactured as ( $11 \times 11 \times 1$  mm, Arrandee™) and deposited over a glass substrate. The further self-organized nanoparticle layer was achieved as follows. We have made the deposition of  $\text{SiO}_2\text{NPs}$  onto Au wafers, *via* 3-MPTS (3-mercaptopropyl triethoxysilane), which is a suitable molecular adhesive linker for the introduction of silica nanoparticles onto gold surfaces. This particular linker is bearing both a thiol and a silane group along a propyl chain, thus enabling  $\text{SiO}_2\text{NPs}$  deposition in an orderly fashion, following previous studies carried out by Vakarelski *et al.*<sup>8</sup>

### 2.2. 3-MPTS coating of Au surfaces

Over a polycrystalline Au layer on glass, a 40 mM solution of 3-MPTS in MeOH was added (366  $\mu\text{L}$ , in 50 mL) then, the wafer was kept immersed for 3 h. Thereafter, the wafer was rinsed with MeOH, dried, and subsequently submerged for 3 h in a freshly prepared solution of 0.01 M NaOH (to induce hydrolysis/polymerization resulting in a Si-O-Si external glass layer). Afterwards, the wafer was again submerged in a pH = 9.0, 1.0 wt%  $\text{SiO}_2$  nanoparticles suspension (500 mg, 50 mL) for 22 hours prior sonication and centrifugation at 3k rpm for 3 minutes. Finally, the sensor was exhaustively rinsed with  $\text{H}_2\text{O}$  mQ and MeOH to exclude the nonspecific binding, and it was allowed to air dry. In the present work, the deposition protocol was implemented as the nanoparticles are doubling in size (200 nm, Fig. S2†). We considered the size of the nanoparticles (200 nm) to be optimal, as we expected to have a nanomaterial showing a balance between (i) aggregation when film-coating (smaller NPs might promote larger self-aggregation) and (ii) effective surface area (larger NPs possess less effective surface area). Also, the thickness of the monolayer plays an important role in the adsorption capacity of the material. In that regard, the immersion step was extended for 22 hours, thus leading to a partially saturation of the Au wafer surface which was confirmed later on by microscopies techniques: Scanning Electron Microscopy (SEM) and Atomic Force Microscopy (AFM).  $\text{CO}_2$  adsorption studies were carried out under well-controlled experimental conditions, inside PASC. The experimental setup is described in the ESI (Fig. S1†). The gold (Au<sub>SiO<sub>2</sub></sub>) surface samples were exposed to an atmosphere of  $\text{CO}_2$  at 7 mbar (similar to the present-day Martian surface conditions) during 22 hours at 25 °C. After being exposed to the  $\text{CO}_2$  atmosphere inside PASC, samples were immediately introduced under high vacuum conditions, and then transferred to ultra-high vacuum conditions for XPS measurements or storage under vacuum conditions before infrared (IR), SEM and AFM analysis.

## 3. Results and discussion

The sensor, comprising a single monolayer of embedded silica nanoparticles loaded over a 1 mm thick gold wafer, was



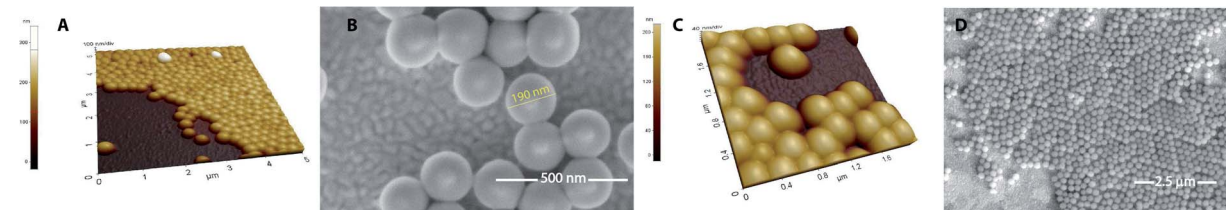


**Fig. 2** AFM (A and C) and SEM ((B) scale bar 500 nm; (D) scale bar 2.5  $\mu$ m) micrographs of 3-MPTS coated Au-wafers submerged 22 h in a  $\text{SiO}_2$  nanoparticle suspension.

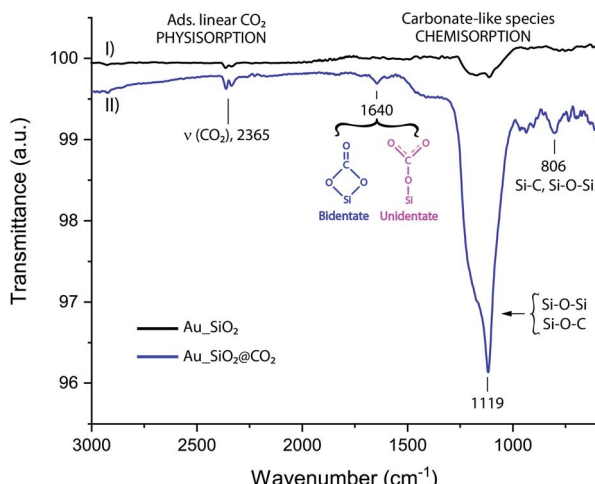


**Fig. 3** IR spectrum of Au wafer bearing  $\text{SiO}_2$  nanoparticles (I) and a gold wafer bearing  $\text{SiO}_2$  nanoparticles after being exposed to  $\text{CO}_2$  atmosphere inside PASC (II)

characterized by several spectroscopic and microscopic techniques before and after  $\text{CO}_2$  exposition. In addition, its theoretical IR spectrum was obtained using computational calculations.

### 3.1. SEM and AFM microscopies

The adsorption and two-dimensional organization of silica nanoparticles ( $\text{SiO}_2$ -NPs) on gold surfaces and its morphological

characterization by SEM, Fig. 2B and D and AFM, Fig. 2A and C, confirmed a well-organized single layer deposition. As expected, there is a time dependence in the coating process, and we have reached a predominant single layer deposition after 22 hours of immersion time. Surprisingly, it is observed that the NPs tend to be adhered between them despite their apparent negative zeta potential at pH = 9.0, hence, a marked repulsion was expected. However, this can be explained with the existence of a hairy (gel-like) external layer, comprising a short, flexible (polymer-like) fragments of poly(silicic acid) attached all over the surface (Fig. S3 and S4<sup>†</sup>).<sup>24-26</sup> The morphology of the nano-structures showed a regular and monodispersed distribution along a NPs row; regarding the surface characteristics of the nanoparticles, it appears to be smooth objects, both in AFM and SEM despite the sol-gel method employed for the synthesis of the nano-compounds, which it is expected to generate some level of “random” porosity. Additional SEM images (Fig. S5<sup>†</sup>) were used to determine the area covered by the nanoparticles. From the number of NPs observed by SEM, the coverage of the monolayer is calculated to be  $55 \pm 5\%$ . This is an excellent result as the deposition was not driven through self-assembly processes. Furthermore, NPs preserve their integrity after deposition as 90% kept the 200 nm size. According to the AFM profile measurements (Fig. S6 and S7<sup>†</sup>), the thickness of the single layer was estimated to be 200 nm, consistent with the NPs size. Novel surface spectroscopic characterization, by reflection adsorption infrared spectroscopy (RAIRS) and X-ray photoelectron spectroscopy (XPS) of these nanostructures, let us establish

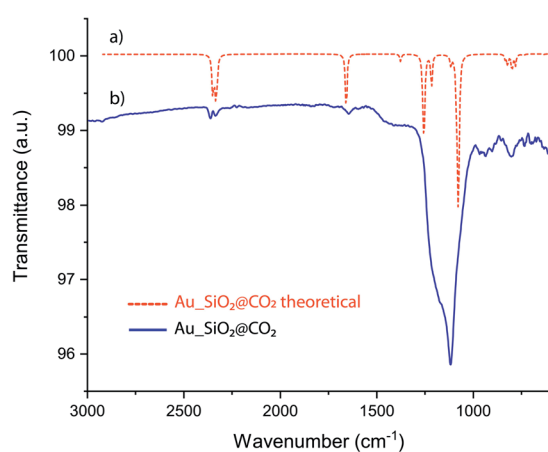
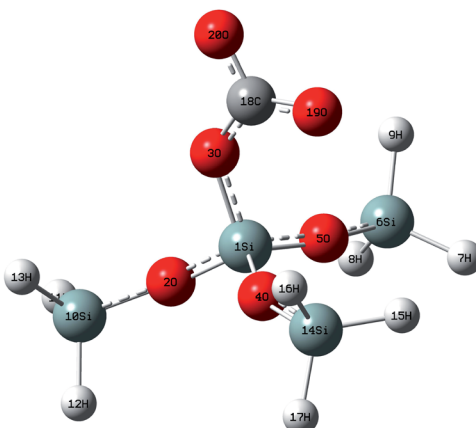


Fig. 4 Schematic illustration of a representative portion of silica surface binding a CO<sub>2</sub>. Superimposed IR spectra of theoretical (a) and experimental (b) Au-SiO<sub>2</sub> when exposed to a CO<sub>2</sub> atmosphere.

their chemical composition after their deposition on the gold surface (Fig. 3-5).

### 3.2. IR spectroscopy

The FTIR was used in this stage of the work to characterize the successful deposition of  $\text{SiO}_2$ NPs on gold surfaces and to identify chemical changes after exposure to the  $\text{CO}_2$  (g) atmosphere. We searched for signatures of the presence of either  $\text{CO}_2$  trapped inside the  $\text{SiO}_2$  pores (physisorption) or covalently anchored in the most plausible form of carbonates (chemisorption). This method allows to also distinguish oxidation process of the  $\text{SiO}_2$ NPs under  $\text{CO}_2$  conditions. FT-IR spectroscopy provides qualitative information about the chemical nature of NPs surface, an important factor when exploring the way, a molecule is interacting and adsorbed on the NPs surface. Fig. 3 shows the superimposed FTIR spectra of  $\text{SiO}_2$ NPs anchored in an Au wafer, before (Fig. 3-I) and after (Fig. 3-II)  $\text{CO}_2$  exposure. The spectrum of pristine  $\text{SiO}_2$  nanoparticles (Au\_SiO<sub>2</sub>, Fig. 3-I) confirms the presence of the antisymmetrical stretching vibration of Si–O–Si at (1010–1130  $\text{cm}^{-1}$ ),<sup>27</sup> hence, the IR technique is suitable for detecting the grafted adsorption of  $\text{SiO}_2$ NPs on gold surface. The spectrum of  $\text{SiO}_2$  nanoparticles (Au\_SiO<sub>2</sub>@CO<sub>2</sub>, Fig. 3-II) after  $\text{CO}_2$  atmosphere exposure inside PASC was also recorded, thus displaying similar IR bands to the ones of “pristine”  $\text{SiO}_2$  nanoparticles; however, in this particular situation, the peaks are narrower and much more intense (1010–1130  $\text{cm}^{-1}$ ), which can be ascribed to the formation of new carbon silica surface bonds, Si–O–C, that falls in the range

of 1150  $\text{cm}^{-1}$ .<sup>28</sup> Furthermore, it is noticeable the presence of two new broad peaks, one at 805  $\text{cm}^{-1}$  that can be attributed to Si–C stretching vibrations and Si–O–Si (symmetrical stretching),<sup>29,30</sup> and a second one, barely seen, at 1640  $\text{cm}^{-1}$  than can be assigned to uni/bidentate carbonates (Si–CO<sub>3</sub>)<sup>31</sup> providing a spectroscopical fingerprint that confirms the successful  $\text{CO}_2$  adsorption process. A control experiment was conducted in order to assess the capacity of  $\text{SiO}_2$ NPs for  $\text{CO}_2$  adsorption, by using a pristine Au wafer in the absence of nanoparticles. Then it was exposed to 7 mbar of  $\text{CO}_2$  inside PASC, concluding that adsorption of  $\text{CO}_2$  is inherent of silica nanoparticles.

### 3.3. Computational details

*Ab initio* calculations of the IR spectra of a representative  $\text{SiO}_2$ NPs (Fig. 4) fragment was calculated, when a  $\text{CO}_2$  molecule is chemisorbed forming a carbonate like group. This was performed with the Gaussian 09W software package, with B3LYP density functional theory (DFT) and basis set 6-311+G(d, p). It is evident the good overlap when superimposing the infrared spectrum of both the theoretical and experimental (Fig. 4), thus confirming the existence of chemisorbed  $\text{CO}_2$  specie in the form of carbonates, over the surface of the NPs. The fragment, here studied, displays a tetrahedral symmetry in the ground state with bond angles values of approximately 109.5°. The vibrational modes registered are mainly symmetrical and antisymmetrical (Fig. S8†) with respect to each of the planes. The theoretical and experimental IR spectra are a perfect match, however a scaling correction factor of 1.06 have been required for DFT values.

(i) Region 3000–1500  $\text{cm}^{-1}$ : the computed DFT analysis predicted CH stretching frequencies (2350  $\text{cm}^{-1}$ ) for the unidentate structure; however, these frequencies can be more likely associated to  $\text{CO}_2$  confinement in the interior of the material.<sup>31</sup> The second region of interest is around 1650  $\text{cm}^{-1}$  that can be ascribed to the umbrella stretching of the chemisorbed R–CO<sub>2</sub> group, a very significant (fingerprint) wave-number value as it confirms the adsorption of the  $\text{CO}_2$  by the matrix.

(ii) Region 1200–900  $\text{cm}^{-1}$ : the bands observed between 1200  $\text{cm}^{-1}$  and 1030  $\text{cm}^{-1}$  are mainly Si–O, Si–O–C and C–O stretches. There is also a small band around 1270  $\text{cm}^{-1}$  that can be attributed to the  $\text{CO}_2$  antisymmetrical stretching.

(iii) Region 800–700  $\text{cm}^{-1}$ : the most intense IR band in this region is located at 790  $\text{cm}^{-1}$ , and it is attributed to the asymmetrical stretches between the Si and O.

### 3.4. XPS analysis

In addition, and with the aim of confirming the appearance of these new chemical species, XPS analysis were performed in the same samples at three different adsorption-process steps: Au\_linker, Au\_SiO<sub>2</sub> and Au\_SiO<sub>2</sub>@CO<sub>2</sub>. XPS is considered to be the most sensitive technique and it is widely used to determine the exact elemental ratio and bonding nature of the elements in NPs materials. The XPS overview spectra of the three different wafers shows that the following atomic species can be identified: O, C, S, Si and Au. Fig. 5 shows the core-level XPS spectra of

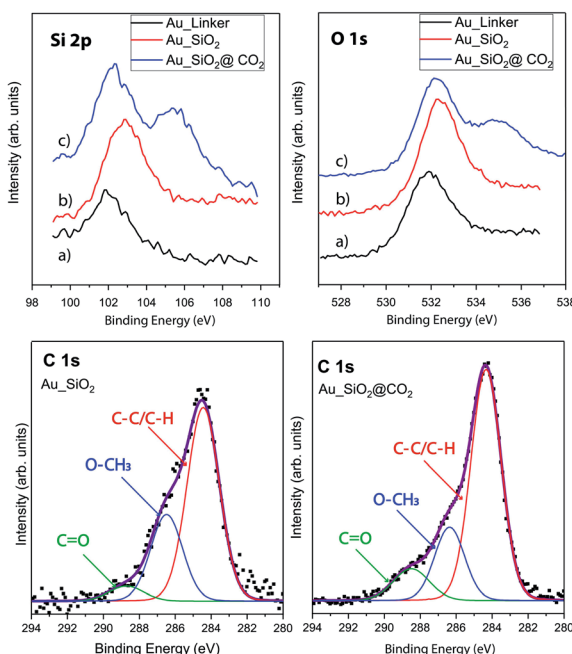


Fig. 5 XPS photoemission spectra of Si 2p and O 1s core level peaks along the three steps of the process on gold surface after: (a) adsorption of linker (Au\_linker), (b)  $\text{SiO}_2$ NPs attachment on gold (Au\_SiO<sub>2</sub>) and (c)  $\text{CO}_2$  exposure (Au\_SiO<sub>2</sub>@CO<sub>2</sub>). Deconvoluted XPS spectra of C 1s before (Au\_SiO<sub>2</sub>) and after (Au\_SiO<sub>2</sub>@CO<sub>2</sub>)  $\text{CO}_2$  exposure.



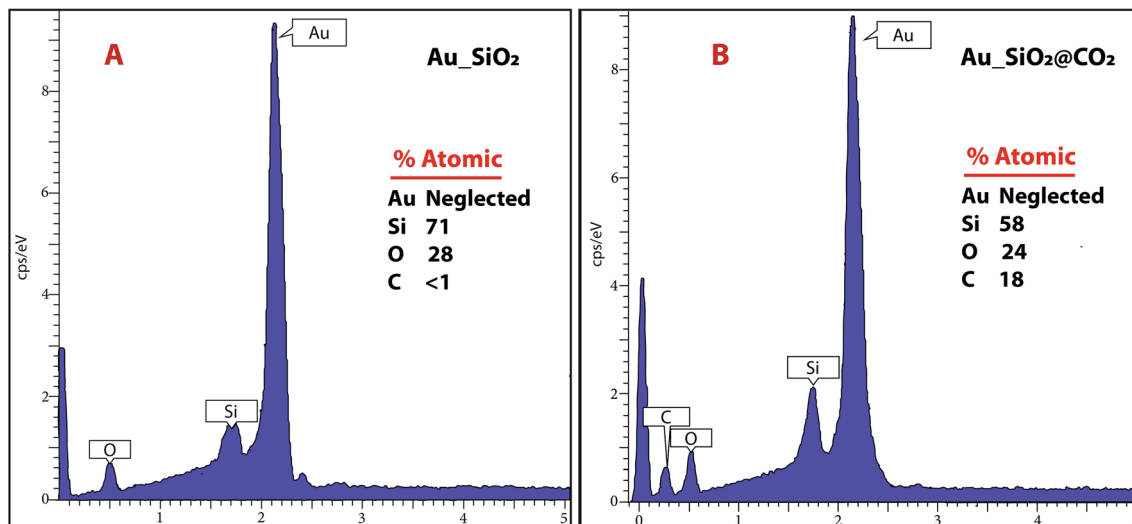


Fig. 6 EDX spectra of (A) the sensor before CO<sub>2</sub> exposure and (B) after CO<sub>2</sub> adsorption.

the O(1s), C(1s) and Si(2p) regions along the three steps of the process. The Si 2p peak is observed at 102.3 eV, and is attributed to Si-C and Si-O species from the chemisorption of the linker (Fig. 5a).<sup>32</sup> In a second step (Fig. 5b), the main peak shows a shift to 102.8 eV in binding energy, related to the SiO<sub>2</sub>NPs adsorption of the gold surface, masking the underneath linker layer. Finally (Fig. 5c), when the sensor is exposed to CO<sub>2</sub>, it gives rise to the appearance of a second component at 105.5 eV, which is ascribed to the presence of electron withdrawing groups<sup>33</sup> on the surface. This fits, in our case, with the formation of Si(CO<sub>3</sub><sup>2-</sup>) species.<sup>34,35</sup> The best-fit curves for the O 1s, depicted in Fig. 5, display a similar trend as silicon, where there is barely a shifting between Au\_linker and Au\_SiO<sub>2</sub> (sensor), then it is noticeable the case of Au\_SiO<sub>2</sub>@CO<sub>2</sub> showing two main components. One is observed at 531.7 eV, attributed to OH and Si-O species, and a second one, in accordance with the silica case, at approximately 535 eV which has been related to C-O containing species.<sup>36-38</sup> Finally, the best-fit curve for the C 1s peak (Fig. 5), in both cases (Au\_SiO<sub>2</sub> and Au\_SiO<sub>2</sub>@CO<sub>2</sub>), was achieved using three components, the first carbon component has a binding energy (B.E.) of 284.5 eV and is attributed to the C-H and C-C group, the second component at 286.4 eV corresponds to O-CH<sub>3</sub> groups whereas the third component is observed at 288.6 eV and is assigned to the C=O groups.<sup>38</sup> There is a remarkable increase in the third component (at 288.6 eV, assigned to the C=O groups), from 5% to 11% (Table S1†) when the Au\_SiO<sub>2</sub> have been exposed to CO<sub>2</sub> which supports the statement of silica nanoparticles as suitable materials for CO<sub>2</sub> adsorption at low pressures. This is in good agreement with the infrared analysis. Both complementary spectroscopies, XPS and infrared, helped us to identify the CO<sub>2</sub> adsorption process and chemical adsorption species, providing a fingerprint signal when the CO<sub>2</sub> fixation process takes place.

### 3.5. EDX analysis

Energy Dispersive X-ray Analysis (EDS or EDX, Fig. 6) technique was used for performing elementary analysis and chemical

characterization of the nanosensor, before (Au\_SiO<sub>2</sub>) and after CO<sub>2</sub> exposure (Au\_SiO<sub>2</sub>@CO<sub>2</sub>), in conjunction with SEM. The impact of the electrons beam on the sensor produces X-rays that are characteristic from the atoms present in the region of study. EDS analysis is then a suitable tool for the determination of the atomic composition of individual spots or for larger areas through a mapping of elements. Based on the results of EDS analysis data, it is possible to conclude that the adsorption of CO<sub>2</sub> is inherent to silica nanoparticles. The atomic percentage of carbon before and after CO<sub>2</sub> exposure, gave the values of about <1 and 18% respectively. This marked increase is ascribed to the formation of chemisorbed carbonates on the surface of the spherical nanoparticles. The electron beam was also pointed in an empty area to assess the intrinsic capacity of the NPs to retain CO<sub>2</sub>, and as expected only the Au peaks were observed in the EDS profile.

## 4. Conclusions

This work show cases the development of an ultra-sensitive sensor, comprised by a well-organized deposition scheme where a monolayer of SiO<sub>2</sub> nanoparticles (200 nm) is efficiently built on a gold (Au) solid substrate, assisted by chemical reactions between NPs and the surface wafer, 3-MPTS mediated. The growth of the monolayer was promoted by the formation of covalent linkages rather than self-assembly processes confirming the importance of the organic linker. This nanosensor can be used as CO<sub>2</sub> gas sensor with excellent sensing performance (12.4 ppm) for CO<sub>2</sub> gas at 7 mbar at room temperature. The sensing response was confirmed by spectroscopies techniques (IR, XPS and EDX) and the morphological features were captured by SEM and AFM microscopies.

These techniques also, provide valuable information regarding the inherent capacity of SiO<sub>2</sub>NPs to capture CO<sub>2</sub>, as atomic EDX analysis can discriminate between the composition of empty and full areas within the wafer.



In conclusion, we have demonstrated that SiO<sub>2</sub>NPs can be self-organized in a two-dimensional ordered structure, which can be fully characterized both spectroscopically and morphologically. Furthermore, we have investigated the suitability of SiO<sub>2</sub>NPs deposited in gold wafers as a tool for CO<sub>2</sub> recognition at standard Mars low pressures. Their low-cost fabrication, small size, and sensitivity (12.4 ppm), opens a new route towards their application in solar system objects possessing very thin atmospheres. These nanosensors could also expand their applications towards the detection of other gasses traces in explored/unexplored solar bodies. The nanosensors could also be used for (i) atmospheric biosignatures detection if referring to the presence of one or several gas species, and (ii) surface biosignatures if detectable by their light reflection characteristics providing spectral molecular fingerprints or characteristic chemical features. Moreover, these results open the door to future studies involving the use of Mars minerals as an atmospheric trap and reservoir. Finally, the aeolian dust which is so characteristic of the Martian atmosphere, has a measured content of about 44% of SiO<sub>2</sub>.<sup>39</sup> This material surface preparation may be used in the future to investigate, within a controlled experimental facility such as PASC, the chemical catalytic reactions that may occur on the surface of mineral aerosols (rich in SiO<sub>2</sub>) in suspension on the Martian CO<sub>2</sub> atmosphere, in contact with other trace molecules, when exposed to the high levels of UV radiation that are characteristic of the Martian atmosphere. In that regard, nanosensors will dramatically improve high-performance materials and contribute to the future space research.

## Conflicts of interest

There are no conflicts to declare.

## Acknowledgements

This work has been supported by the MINECO project ESP2017-89053. The Instituto Nacional de Técnica Aeroespacial supported the work performed at Centro de Astrobiología (CAB). This project has been partially funded by the Spanish State Research Agency (AEI) Project No. MDM-2017-0737 Unidad de Excelencia "María de Maeztu"-Centro de Astrobiología (INTA-CSIC). E. C. D. Postdoctoral Fellowship from CAM reference: 2018/TIC-10616. We thank you M. Sampedro for IR technical support. E. M. M. has been partially supported by Spanish Ministry of Science and Innovation project (ref. PID2019-104205GB-C21).

## Notes and references

- 1 E. Ljunggren and B. Karlberg, *J. Autom. Chem.*, 1995, **17**, 780672.
- 2 B. H. Weigl and O. S. Wolfbeis, *Sens. Actuators, B*, 1995, **28**, 151–156.
- 3 T. Beuermann, D. Egly, D. Geoerg, K. I. Klug, W. Storhas and F.-J. Methner, *J. Biosci. Bioeng.*, 2012, **113**, 399–405.
- 4 D. Zhao, D. Miller, X. Xian, F. Tsow and E. S. Forzani, *Sens. Actuators, B*, 2014, **195**, 171–176.
- 5 J.-W. Kim, H.-S. Hong and C.-O. Park, *Sens. Lett.*, 2008, **6**, 868–872.
- 6 R. Ali, S. M. Saleh, R. J. Meier, H. A. Azab, I. I. Abdalgawad and O. S. Wolfbeis, *Sens. Actuators, B*, 2010, **150**, 126–131.
- 7 Z. Liu, C. Zheng, C. Chen, H. Xie, Q. Ren, W. Ye, Y. Wang and F. K. Tittel, *Anal. Methods*, 2018, **10**, 4838–4844.
- 8 I. U. Vakarelski, C. E. McNamee and K. Higashitani, *Colloids Surf. A*, 2007, **295**, 16–20.
- 9 S. Naama, T. Hadjersi, A. Keffous and G. Nezzal, *Mater. Sci. Semicond. Process.*, 2015, **38**, 367–372.
- 10 A. M. Alwan and A. B. Dheyab, *Appl. Nanosci.*, 2017, **7**, 335–341.
- 11 P. Viswanathan, A. K. Patel, J. Pawar, A. Patwardhan and R. Henry, *IETE J. Res.*, 2018, 1–6, DOI: 10.1080/03772063.2018.1502625.
- 12 N. B. Tanvir, C. Wilbertz, S. Steinhauer, A. Köck, G. Urban and O. Yurchenko, *Mater. Today: Proc.*, 2015, **2**, 4190–4195.
- 13 Y. Liu, M. G. Williams, T. J. Miller and A. V. Teplyakov, *Thin Solid Films*, 2016, **598**, 16–24.
- 14 S. Nilsson, Master's thesis, Chalmers University of Technology, 2016, <https://www.semanticscholar.org/paper/Exploring-Colloidal-Silica-Nanoparticles-for-Carbon-Nilsson/26450c00a86af8ea46c30861cca8e60c345ad298>.
- 15 J. Boudaden, A. Klumpp, H.-E. Endres and I. Eisele, *Nanomaterials*, 2019, **9**, 1097.
- 16 S. Meth, A. Goeppert, G. K. S. Prakash and G. A. Olah, *Energy Fuels*, 2012, **26**, 3082–3090.
- 17 T. C. D. Doan, R. Ramaneti, J. Baggerman, J. F. van der Bent, A. T. M. Marcelis, H. D. Tong and C. J. M. van Rijn, *Sens. Actuators, B*, 2012, **168**, 123–130.
- 18 T. C. D. Doan, J. Baggerman, R. Ramaneti, H. D. Tong, A. T. M. Marcelis and C. J. M. van Rijn, *Sens. Actuators, B*, 2014, **201**, 452–459.
- 19 K. S. Rao, K. El-Hami, T. Kodaki, K. Matsushige and K. Makino, *J. Colloid Interface Sci.*, 2005, **289**, 125–131.
- 20 W. Stöber, A. Fink and E. Bohn, *J. Colloid Interface Sci.*, 1968, **26**, 62–69.
- 21 Z.-U. L. A. Arain, S. Al-Anssari, M. Ali, S. Memon, M. A. Bhatti, C. Lagat and M. Sarmadivaleh, *Petroleum*, 2019, DOI: 10.1016/j.petlm.2019.09.001.
- 22 E. Mateo-Martí, O. Prieto-Ballesteros, J. M. Sobrado, J. Gómez-Elvira and J. A. Martín-Gago, *Meas. Sci. Technol.*, 2006, **17**, 2274–2280.
- 23 M. F. Simões, C. A. Ottoni and A. Antunes, *Life*, 2020, **10**, 28.
- 24 G. Vigil, Z. Xu, S. Steinberg and J. Israelachvili, *J. Colloid Interface Sci.*, 1994, **165**, 367–385.
- 25 J. Israelachvili and H. Wennerström, *Nature*, 1996, **379**, 219–225.
- 26 M. Kobayashi, F. Juillerat, P. Galletto, P. Bowen and M. Borkovec, *Langmuir*, 2005, **21**, 5761–5769.
- 27 S. C. Feifel and F. Lisdat, *J. Nanobiotechnol.*, 2011, **9**, 59.
- 28 A. S. Zakirov, R. Navamathavan, Y. J. Jang, A. S. Jung, K.-M. Lee and C. K. Choi, *J. Korean Phys. Soc.*, 2007, **50**, 1809.
- 29 R. F. S. Lenza and W. L. Vasconcelos, *Mater. Res.*, 2001, **4**, 175–179.



30 H. Liu, Z. Huang, J. Huang, M. Fang, Y.-g. Liu and X. Wu, *J. Mater. Chem. C*, 2014, **2**, 7761–7767.

31 M. Santoro, F. Gorelli, J. Haines, O. Cambon, C. Levelut and G. Garbarino, *Proc. Natl. Acad. Sci. U. S. A.*, 2011, **108**, 7689.

32 A. Morneau, A. Manivannan and C. R. Cabrera, *Langmuir*, 1994, **10**, 3940–3942.

33 E. Botha, M. Landman, P. H. van Rooyen and E. Erasmus, *Inorg. Chim. Acta*, 2018, **482**, 514–521.

34 F. Han, S. Yang, W. Jing, K. Jiang, Z. Jiang, H. Liu and L. Li, *Opt. Express*, 2014, **22**, 11436–11445.

35 C.-J. Weng, C.-H. Chang, C.-W. Peng, S.-W. Chen, J.-M. Yeh, C.-L. Hsu and Y. Wei, *Chem. Mater.*, 2011, **23**, 2075–2083.

36 A. v. Cresce, S. M. Russell, D. R. Baker, K. J. Gaskell and K. Xu, *Nano Lett.*, 2014, **14**, 1405–1412.

37 C. Shen, G. Hu, L.-Z. Cheong, S. Huang, J.-G. Zhang and D. Wang, *Small Methods*, 2018, **2**, 1700298.

38 R. Sujith, P. K. Chauhan, J. Gangadhar and A. Maheshwari, *Sci. Rep.*, 2018, **8**, 17633.

39 J. Lasue, A. Cousin, P. Y. Meslin, N. Mangold, R. C. Wiens, G. Berger, E. Dehouck, O. Forni, W. Goetz, O. Gasnault, W. Rapin, S. Schroeder, A. Ollila, J. Johnson, S. Le Mouélic, S. Maurice, R. Anderson, D. Blaney, B. Clark, S. M. Clegg, C. d'Uston, C. Fabre, N. Lanza, M. B. Madsen, J. Martin-Torres, N. Melikechi, H. Newsom, V. Sautter and M. P. Zorzano, *Geophys. Res. Lett.*, 2018, **45**, 10968–10977.

